

<https://doi.org/10.1038/s43247-025-03047-w>

A meta-coupling analysis between three-dimensional urbanization and ecosystem services in China's urban agglomerations

Check for updates

Yinshuai Li^{1,2}, Nan Jia^{3,4,5} ✉, Lilin Zheng^{1,2}, Chenglong Yin⁶, Kai Chen^{1,2}, Nansha Sun^{1,2}, Anyao Jiang^{1,2}, Mengting Wang⁷, Ruishan Chen^{1,2} ✉ & Zhenju Zhou⁸

Rapid urbanization exacerbates conflicts between land expansion and ecosystem preservation, particularly in urban agglomerations, posing challenges to sustainable urban development. Nevertheless, existing research often overlooks the three-dimensional urbanization process. Here we established a framework for coupling coordination degree analysis based on meta-coupling theory to explore relationships between three-dimensional urbanization (both horizontal and vertical dimensions) and multiple ecosystem services, using 19 major urban agglomerations in China from 2005 to 2020 as case studies. The results reveal that, although the coupling coordination degree has generally improved, some urban agglomerations (e.g., Chengdu-Chongqing and Qianzhong) have experienced degradation, and several western and inland regions show persistent or worsening imbalances. Differences between regions are the main contributors to overall variation, yet cross-regional coupling coordination is strengthening. These findings underscore the importance of strengthening inter-regional cooperation by leveraging the spillover influence of advanced cities to support resource sharing—such as ecological data, technology, and restoration funding—and policy alignment in land-use planning and ecological compensation, thereby supporting more balanced and sustainable development.

Over the past four decades, China has experienced a rapid urbanization process, with the urbanization rate rising from 17.92% in 1978 to 65.22% in 2022¹. With this process, the expansion of urban spaces—especially the impervious surfaces—has reshaped human-environment interactions and altered the structure and function of regional ecosystems^{2,3}. These changes will threaten the sustainable supply of ecosystem services (ES), namely the various benefits that natural ecosystems provide to humanity⁴.

The concept of ES encompasses provisioning (e.g., food and water), regulating (e.g., climate regulation and air quality maintenance), supporting (e.g., erosion prevention and habitat provision), and cultural services (e.g., recreational and esthetic values), and their values can be quantified through ecosystem service values (ESVs)^{5,6}. To measure ESVs, researchers employ various methods, including biophysical assessments (e.g., the InVEST model, functional value method, and indicator proxy method), monetary

valuation approaches (e.g., the SOLVES model and hedonic pricing), and the emergy valuation method⁷. Applying these methods, numerous studies have shown that rapid urban expansion has replaced natural ecosystems with built-up areas, thereby weakening various ecological service functions^{8,9}. For instance, Yuan et al.¹⁰ found that the growth of built-up land has caused declines in food production, water conservation, climate regulation, habitat support, and cultural services, estimating that urban expansion in China from 1985 to 2015 caused an ES loss of USD 110.95 billion. Additionally, Xie et al.¹¹ predict that urban expansion in Beijing from 2013 to 2040 will result in decreases of 20.70%, 8.69%, 6.45%, 5.76%, and 3.92% in food production, water conservation, habitat quality, carbon storage, and air quality regulation, respectively. Given the dependence of urban development on natural resources and environmental conditions, maintaining and enhancing ES has become a critical challenge for sustainable development¹². These

¹School of Design, Shanghai Jiao Tong University, Shanghai, China. ²Digital Engineering Technology Innovation Center for Territorial Ecological Governance, Ministry of Natural Resources, Shanghai, China. ³College of Public Administration, Nanjing Agricultural University, Nanjing, China. ⁴Center for Systems Integration and Sustainability, Department of Fisheries and Wildlife, Michigan State University, East Lansing, MI, USA. ⁵Centre for Geographic Analysis, Harvard University, Cambridge, MA, USA. ⁶College of Geography and Environment, Shandong Normal University, Jinan, China. ⁷Ningbo Key Laboratory of Agricultural Germplasm Resources Mining and Environmental Regulation, College of Science and Technology, Ningbo University, Cixi, China. ⁸Department of Natural Resources of Xinjiang Uygur Autonomous Region, Urumqi, China. ✉e-mail: cannonjia17@gmail.com; rschen@sjtu.edu.cn

conflicts underscore the importance of balancing urban growth with ES conservation, particularly in rapidly urbanizing regions (e.g., urban agglomerations).

Urban agglomerations, as the foundation of China's new-type urbanization strategy and an advanced form, are distinguished from single cities by their polycentric structure of interconnected city systems, shaped by the flows of people, resources, and information across urban boundaries¹³. Statistics reveal that these regions now concentrate 68.54% of China's fixed-asset investments and nearly all foreign capital (98.06%), yet simultaneously bear over 75% of the national pollution emissions¹⁴. Recent studies by Zhai et al.¹⁵, Ding et al.¹⁶, and Li et al.¹⁷ have analyzed the relationship changes between urbanization and ES in major agglomerations such as the Beijing-Tianjin-Hebei, Yangtze River Delta, and Lanzhou-Xining. However, a limitation of these studies is that they only focus on horizontal urban expansion, which overlooks the crucial role of vertical urbanization in shaping urban growth and its ecological effects. Specifically, horizontal and vertical urbanization jointly reshape land-use intensity and spatial configuration, influencing various ES through different mechanisms¹⁸. For instance, increased building density (horizontal) and height (vertical) modify microclimates and energy fluxes, thereby affecting climate regulation; reduced green and permeable surfaces alter hydrological regulation; landscape fragmentation disrupts habitat and supporting services; and changes in accessibility and visual environments affect cultural services^{19,20}. Therefore, it is necessary to incorporate 3D urban expansion into related research.

Additionally, when studying the relationships between urbanization and ES, previous research has shown that it is often difficult to use process-based models at large spatial scales due to data limitations and high parameterization requirements. Instead, many studies have adopted indicator-based approaches to represent urbanization dynamics—such as changes in impervious surface area or building height^{18–20}—and ecosystem service functions—such as ESVs equivalents based on land use types—in a simplified but robust way^{8,9}. Under this indicator-based approach, the coupling coordination degree (CCD) model offers a valuable framework for capturing the coupling intensity and development coordination between systems, drawing on the principles of system evolution²¹. For instance, Qiao et al.²² examined the interactive coupling functions, trajectories, types, and stages between urbanization and ecological environments. Their case study in arid regions demonstrated a dynamic coupling relationship characterized by mutual reinforcement under interactive stress. Additionally, Ai et al.²³ and Zhu et al.²⁴ utilized CCD models to evaluate the coupling coordination relationships between urbanization and ES across different cities. However, these works predominantly focus on intra-urban dynamics while overlooking cross-regional ecological linkages, particularly how cities externalize environmental costs through distant resource extraction (e.g., food/energy imports) and pollution displacement, potentially depleting sender systems and degrading recipient ecosystems^{25,26}. Specifically, the polycentric, networked development model of urban agglomerations—characterized by factor mobility, industrial clustering, and functional complementarity—presents fundamental challenges to traditional local-scale analysis frameworks due to its complex spatial interactions and ecosystem interdependencies. Fortunately, Liu's^{27,28} meta-coupling framework provides a comprehensive analytical lens for understanding complex human-environment coupling relationships. While originally applied to global trade and invasive species^{29,30}, this approach also offers potential for understanding cross-scale relationships between urbanization and ES.

This study established a multi-scale coupling coordination analysis framework based on a meta-coupling framework to systematically examine the interactive relationship between 3D urbanization and ESVs during China's rapid urbanization process. The research aims to fill current knowledge gaps regarding cross-regional synergies, while providing a scientific basis for coordinating regional sustainable development. Building on this framework, we propose the following key research questions: (1) From a 3D spatial perspective, what are the spatiotemporal differentiation characteristics of urbanization across China's urban agglomerations? How do

different ESVs evolve, and what are their similarities and differences? (2) How do 3D urbanization and ESVs create differentiated coupling coordination patterns through intra-coupling (within individual cities), pericoupling (within urban agglomerations), and tele-coupling (between different urban agglomerations), and how can these coupling coordination relationships contribute to the synergistic optimization between them?

Results

Spatiotemporal evolution of 3D urbanization in China's urban agglomerations

Urbanization in horizontal and vertical dimensions. From a horizontal perspective (Fig. 1a, d, and Supplementary Table S2), all urban agglomerations experienced continuous spatial expansion during the study period. The average Horizontal Urbanization Intensity Index (HUII) increased from 0.038 in 2005 to 0.087 in 2020. By 2020, the highest HUII value (0.545) was observed in Dongguan City in PRD, while Hainan Tibetan Autonomous Prefecture City in LX was the lowest (0.002), reflecting pronounced differences in regional urbanization. Among numerous urban agglomerations, the PRD consistently led horizontal expansion, while the YRD surpassed the BTH after 2010, and by 2020, the SP also exceeded the BTH (0.172). In contrast, most other agglomerations, particularly those west of the CP, maintained average HUII values below 0.05, indicating relatively lagging horizontal urbanization.

In the vertical dimension (Fig. 1b, e, Supplementary Fig. S1, and Supplementary Table S3), building height growth was more modest, indicating that horizontal expansion remains the dominant urbanization pattern. The average Vertical Urbanization Intensity Index (VUII) of some cities has stagnant or even declining trends. In 2020, Shenzhen City in PRD reached the peak VUII (0.151), while Huyanghe City in TNS was the lowest (0.058). Notably, earlier leaders in vertical urbanization, such as CC and QZ, declined to average values of 0.096 and 0.099 in 2020, respectively. The PRD demonstrated continuous vertical growth, particularly in Shenzhen, Zhuhai, Dongguan, and Guangzhou. Meanwhile, other agglomerations exhibited relatively slow vertical development.

3D urbanization. To address potential multicollinearity between the HUII and VUII used in constructing the 3D Urbanization Intensity Index (3D-UUI), we calculated the variance inflation factor (VIF) for each study period. The results showed that all VIF values were below 10, indicating no multicollinearity (Supplementary Table S4). By integrating horizontal and vertical dimensions, the results reveal that cities and urban agglomerations in the southeastern coastal regions and the Yangtze River Basin exhibited prominent 3D urbanization, particularly Shenzhen, Dongguan, and Shanghai. In contrast, the northern and western cities lagged (Fig. 1c and Supplementary Fig. S2). Temporally, the overall 3D urbanization continuously increased, with the average 3D-UUI rising from 0.225 to 0.266. By 2020, the highest 3D-UUI (0.930) was observed in Shenzhen City in PRD, while Huyanghe City in TNS reached the lowest value (0.060). Specifically, the PRD consistently led and continued to improve, with an initial average 3D-UUI of 0.434 that already exceeded the 2020 levels of most other urban agglomerations. In contrast, the QZ and CC, both initially ranked high, experienced notable declines, with average values decreasing to 0.251 and 0.274 in 2020, respectively. Additionally, most other urban agglomerations showed upward trends, such as the BTH, where the average values increased from 0.178 to 0.282, and the YRD, which increased from 0.242 to 0.390 (Fig. 1f and Supplementary Table S5).

Spatiotemporal evolution of ESVs in China's urban agglomerations

The total ESV exhibited a spatial distribution pattern of higher in the east than the west, and higher in the south than the north (Fig. 2a and Supplementary Fig. S3). During the study period, the average total ESV across the 19 urban agglomerations declined from 7.860 billion yuan/km² in 2005 to

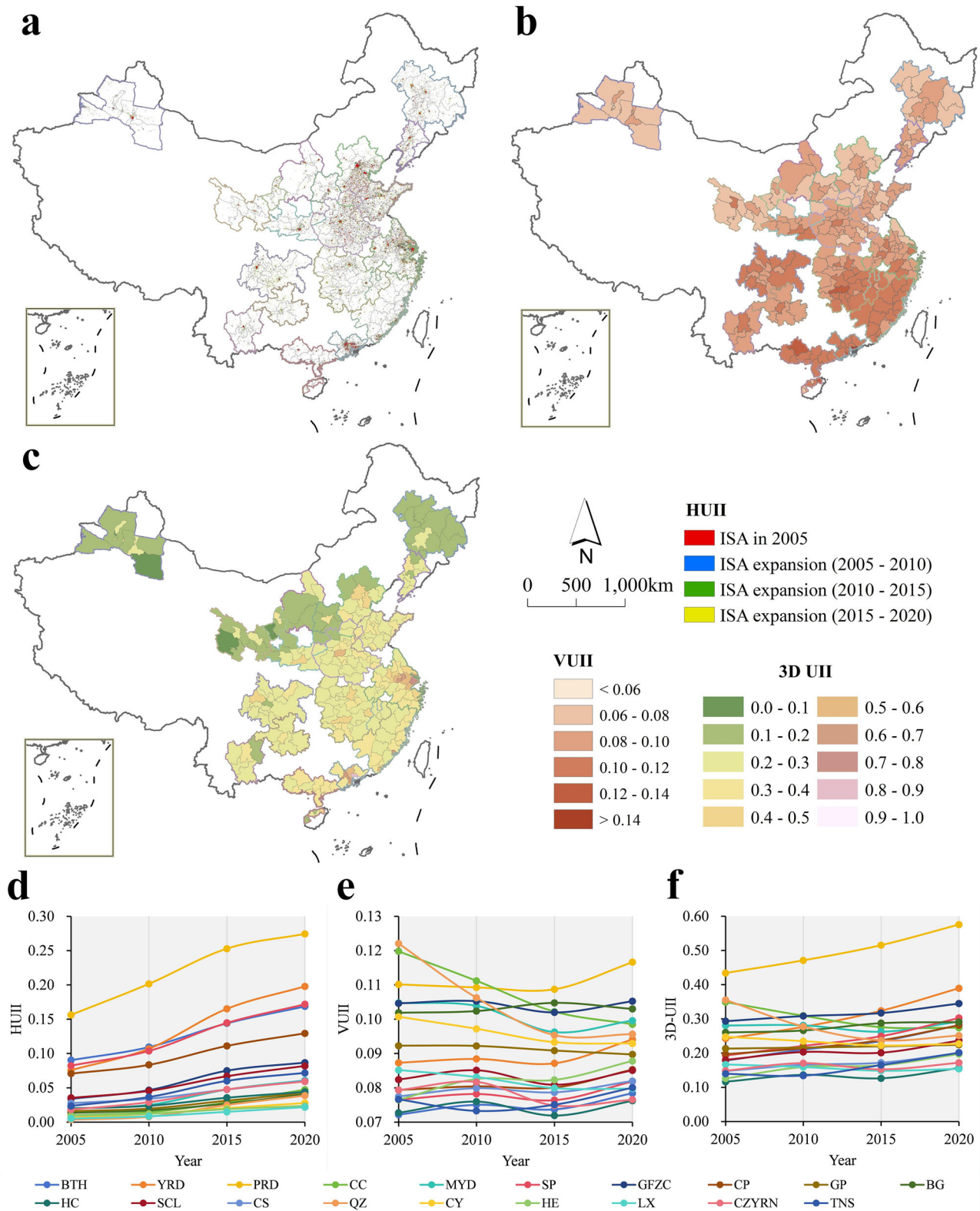


Fig. 1 | Spatiotemporal patterns of 3D urbanization in China's urban agglomerations. **a** The horizontal expansion of impervious surface area (ISA). The spatial patterns of vertical (**b**) and 3D urbanization (**c**) in 2020 (see Supplementary Figs. S1 and S2 for the results in 2005, 2010, and 2015). The dynamic changes of

average HUII (**d**), VUII (**e**), and 3D-UUI (**f**) across urban agglomerations from 2005 to 2020. The full names of urban agglomerations can be found in Supplementary Table S1. In addition, detailed descriptive statistical results for each urban agglomeration are available in Supplementary Tables S2, S3, and S5.

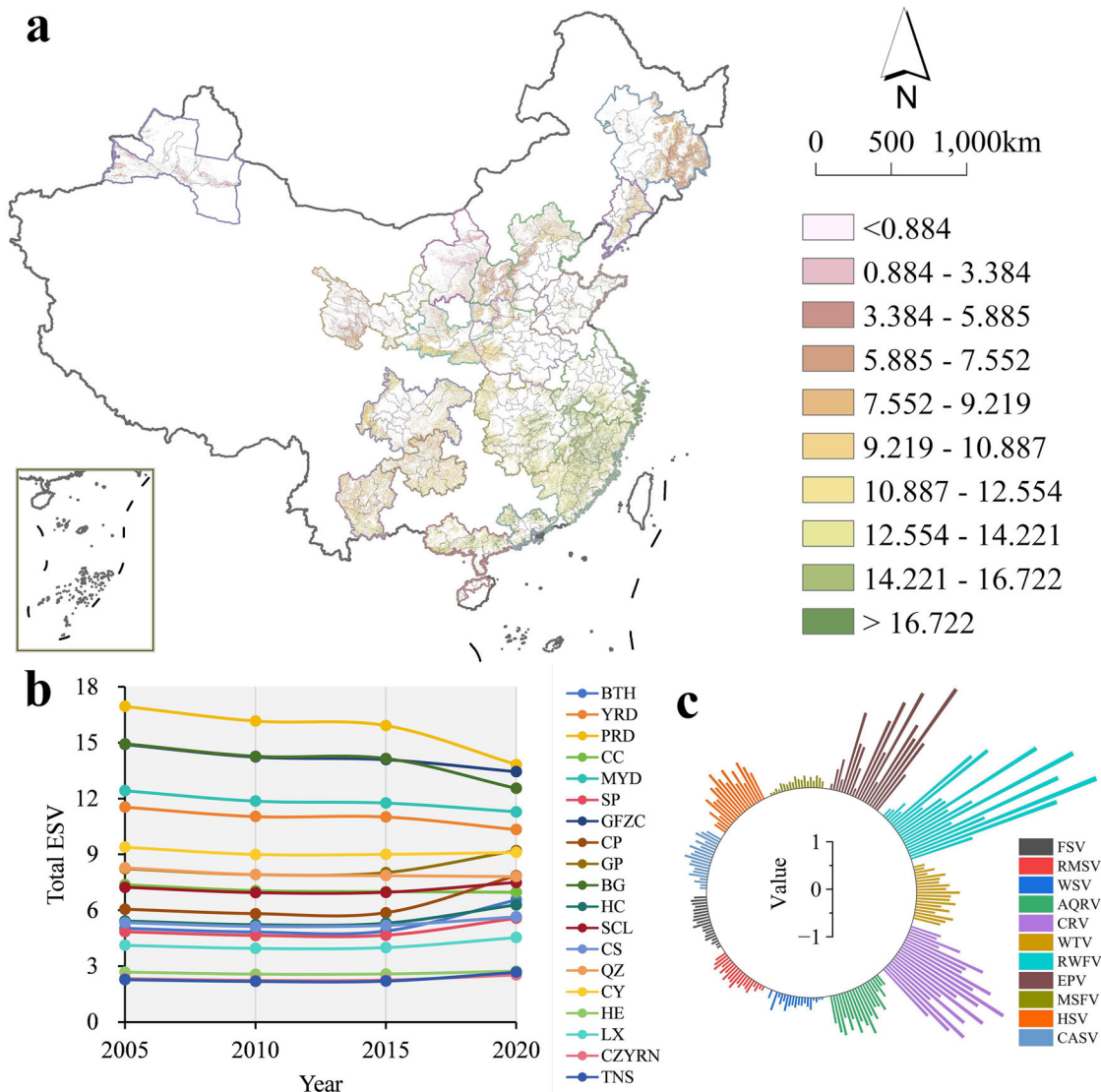


Fig. 2 | Spatiotemporal patterns of ESVs in China’s urban agglomerations. **a** The spatial patterns of the total ESV in 2020 (see Supplementary Fig. S3 for the results in 2005, 2010, and 2015). **b** The dynamic changes of the average total ESV across urban agglomerations from 2005 to 2020. **c** The average values of the 11 ESVs in 2020, with urban agglomerations arranged counterclockwise as the BTH, YRD, PRD, CC, MYD, SP, GFZC, CP, GP, BG, HC, SCL, CS, QZ, CY, HE, LX, CZYRN, and TNS. The

full names are provided in Supplementary Table S1. In addition, detailed descriptive statistical results for the total ESV in each urban agglomeration are available in Supplementary Table S6, while the spatial distributions and other detailed descriptive statistical results for all 11 ESVs can be found in Supplementary Figs. S4–S9.

7.511 billion yuan/km² in 2015, before rebounding to 7.707 billion yuan/km² in 2020—though still below initial levels. In 2020, the maximum values (21.966 billion yuan/km²) were observed in Bozhou City in CP, while the minimum values (1.144 billion yuan/km²) were observed in TNS (Fig. 2b and Supplementary Table S6).

Among individual service categories, most ESVs have similar spatial distribution differences as observed in the total ESV (Supplementary Figs. S4–S7). During the study period, FSV, RWFV, and MSFV showed continuous declines, with their average values decreasing from 0.292, 2.124, and 0.190 billion yuan/km² to 0.240, 1.811, and 0.158 billion yuan/km², respectively. Additionally, other service indicators also showed an initial decline followed by a recovery, which was similar to the total ESV (Fig. 2c, Supplementary Figs. S8 and S9).

Specifically, the total ESV in PRD, GFZC, and BG maintained relatively high values but showed consistent declines over time, suggesting potential ecosystem degradation risks. In contrast, the HE, CZYRN, and TNS demonstrated improvement from initially low baselines, although their

maximum values in 2020 (5.600 billion yuan/km²) were still below the minimum values in many other urban agglomerations in 2005. In addition, similar patterns were observed for other service indicators (Fig. 2, Supplementary Figs. S3–S9, and Supplementary Table S6).

The multi-scale coupling coordination relationship between 3D urbanization and ESVs

Intra-coupling coordination relationship. Overall, the CCD between 3D urbanization and the total ESV improved slightly, shifting from being at the edge of being uncoordinated (average intra-CCD = 0.485) to barely coordinated (average intra-CCD = 0.506). Simultaneously, among 11 service categories, only WSV reached a slightly coordinated state, while most others remained at the edge of being uncoordinated or barely coordinated. Spatially, eastern and southern cities exhibited higher intra-CCD values, predominantly reaching barely, slightly, or moderately coordinated, with some cities, such as Shenzhen and Zhuhai in PRD, even achieving well-coordinated or perfectly coordinated. Central cities

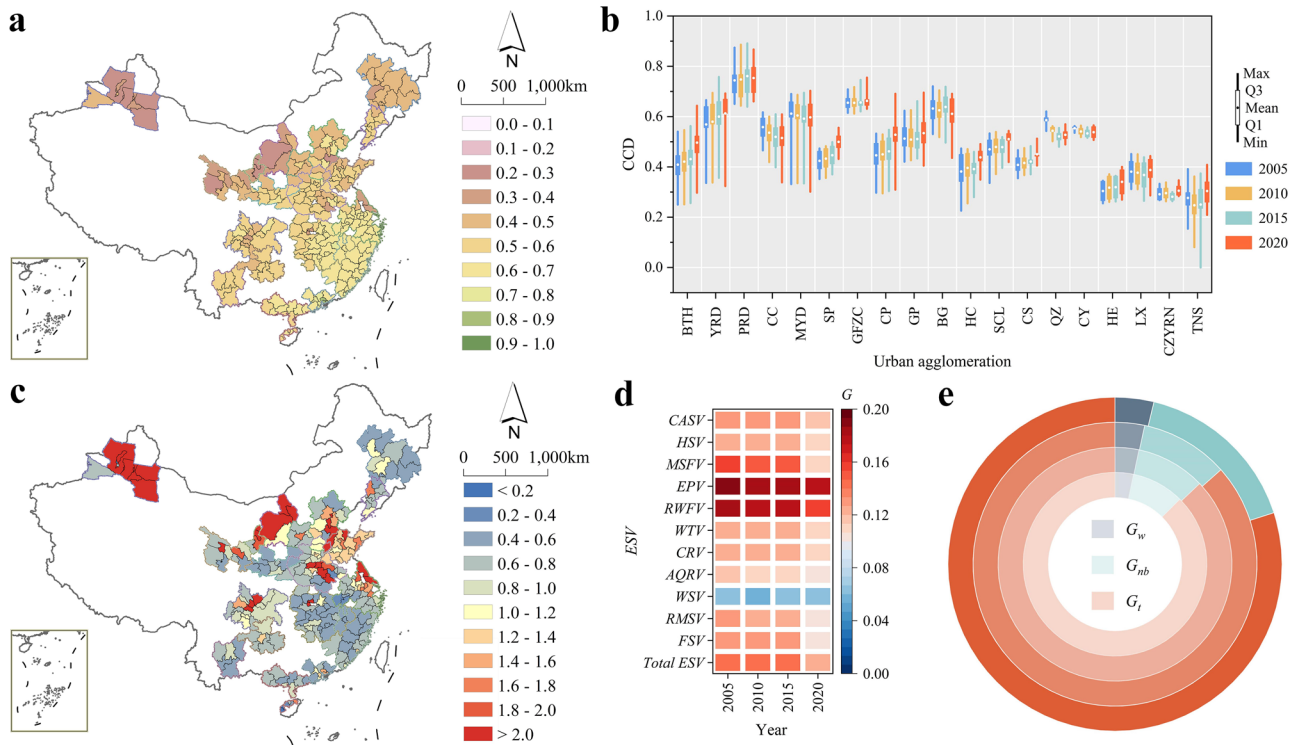


Fig. 3 | Intra-CCD between 3D urbanization and ESVs in China's urban agglomerations. **a** The spatial patterns of intra-CCD between 3D urbanization and the total ESV in 2020 (see Supplementary Fig. S10 for the results in 2005, 2010, and 2015). **b** The changes of intra-CCD between 3D urbanization and the total ESV in different urban agglomerations. **c** The relative development levels between 3D urbanization and the total ESV for individual cities in 2020 (see Supplementary Fig. S11 for the results in 2005, 2010, and 2015). **d** The temporal trends of overall Gini

coefficients measuring intra-CCD differences between multiple ESVs and 3D urbanization across urban agglomerations. **e** The sources of differences and the changes of contribution rates for intra-CCD between 3D urbanization and the total ESV, with concentric rings from center to edge representing the contribution rates of G_w , G_{nb} , and G_t in 2005, 2010, 2015, and 2020, respectively. The full names are provided in Supplementary Table S1. In addition, detailed results for other service indicators are available in Supplementary Figs. S12–S22.

exhibited relatively lower intra-CCD values, often at the edge of being uncoordinated or slightly coordinated, whereas northern and western cities demonstrated the lowest coordination levels, often at the edge of being uncoordinated or slightly uncoordinated. Notably, Shihezi and Shizuishan City in TNS fall into moderately or seriously uncoordinated status (Fig. 3a, Supplementary Figs. S10, S12–S22).

Specifically, the PRD, GFZC, and BG showed relatively high intra-coupling coordination between 3D urbanization and the total ESV, with many cities achieving at least barely coordinated. In contrast, numerous cities in TNS, CZYRN, and HE remained in slightly uncoordinated states. Simultaneously, the intra-CCD values of most urban agglomerations showed increasing trends during the study period, although CC and QZ experienced notable declines (Fig. 3b). Among 11 service categories, most urban agglomerations remained in coordinated states. Notably, several first-tier urban agglomerations, particularly CC, displayed declining intra-CCD values across various ESVs, suggesting potential negative impacts of urbanization on local ES.

In addition, relative development analysis revealed that most eastern and southern cities had ESVs exceeding their urbanization development, indicating relatively strong ecological support for rapid urbanization. However, the opposite pattern was observed in central (e.g., CC and CP), certain eastern (e.g., SP, BTH, and CP), and northern (e.g., LX, CZYRN, HE, and TNS) regions, with urbanization surpassing ESVs despite lower absolute urbanization levels compared to eastern or southern regions (Fig. 3c, Supplementary Figs. S11, and S12–S22). Further analysis based on the Dagum Gini coefficient indicated that intra-CCD values for multiple ESVs ranged from 0.059 to 0.187, with the overall differences gradually narrowed over time. For instance, the Gini coefficient for the intra-CCD between 3D urbanization and the total ESV decreased from 0.145 to 0.123 (Fig. 3d). Furthermore, decomposition results of the Gini coefficients revealed that G_{nb}

(inter-regional net differences) is the main source of G (overall Gini coefficient), contributing 80.290–96.557%, followed by G_t (intensity of transvariation, 1.820–16.332%), and G_w (intra-regional differences) contributed the least (1.560–3.377%) (Fig. 3e and Supplementary Figs. S12–S22).

Peri-coupling coordination relationship. Overall, the peri-CCD values between 3D urbanization and multiple ESVs improved over time. For instance, the average peri-CCD between 3D urbanization and the total ESV was initially at the edge of being uncoordinated (0.487), but increased to barely coordinated (0.511) by 2020. Among 11 service categories, only WSV reached a slightly coordinated status with 3D urbanization, while most others remained at the edge of being uncoordinated or barely coordinated (Fig. 4a and Supplementary Fig. S23).

Concerning the coupling coordination relationship between 3D urbanization and the total ESV, multiple urban agglomerations, including BTH, YRD, SP, CS, and HE, exhibited rising trends, while noticeable declines were observed in CC, QZ, and CY from 2005 to 2020. Specifically, the PRD exhibited the highest peri-CCD values, with most cities achieving moderately coordinated or well-coordinated. Simultaneously, the GFZC and BG generally reached slightly or moderately coordinated with limited variation, indicating relatively balanced peri-coupling coordination. Conversely, urban agglomerations, such as HE, LX, CZYRN, and TNS, remained in a moderately or slightly uncoordinated state (Fig. 4a).

Furthermore, among 11 service categories, most urban agglomerations achieved coordinated peri-CCD states with 3D urbanization. However, in HE, LX, CZYRN, and TNS, all indicators except WSV remained slightly or moderately uncoordinated with 3D urbanization, but fortunately, improvements were evident over time. Notably, declining peri-CCD trends were also observed for most ESVs in CC and QZ, as well as for FSV, RMSV, and MSFV in urban agglomerations such as PRD, MYD, GEZC, BG, and

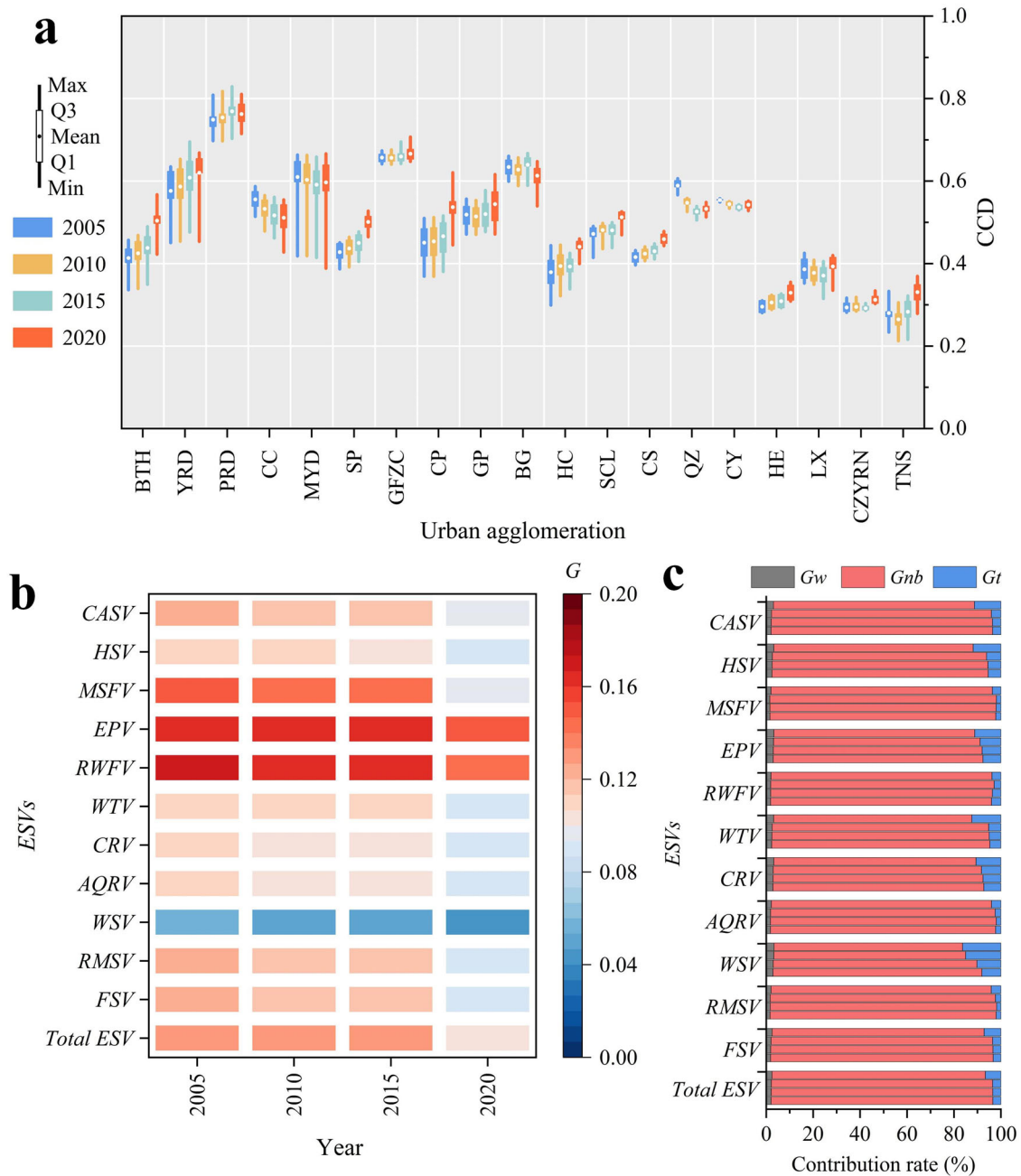


Fig. 4 | Peri-CCD between 3D urbanization and ESVs in China's urban agglomerations. **a** The changes of peri-CCD between 3D urbanization and the total ESV in different urban agglomerations (see Supplementary Fig. S23 for the results of other service indicators). **b** The temporal trends of overall Gini coefficients measuring peri-CCD differences between multiple ESVs and 3D urbanization across

urban agglomerations. **c** The sources of differences and the changes of contribution rates for peri-CCD, with results for 2005, 2010, 2015, and 2020 shown from bottom to top in each service categories. The full names are provided in Supplementary Table S1.

CY (Supplementary Fig. S23). Additionally, there are notable differences ($G > 0.097$) in peri-CCD between RWFV, EPV, MSFV, and 3D urbanization, but these differences narrowed consistently, indicating that the overall coupling coordination relationship with surrounding areas tends to be balanced (Fig. 4b). Further decomposition of the Gini coefficients revealed that G_{nb} is the main source of G , contributing over 80.29% on average. However, its contribution rate gradually decreased over time (Fig. 4c).

Tele-coupling coordination relationship. Overall, the tele-CCD between 3D urbanization and multiple ESVs has also improved over time. For instance, the average tele-CCD between 3D urbanization and the total ESV increased from 0.502 to 0.526. Among 11 service categories

by 2020, RMSV, AQRV, CRV, HSV, and CASV had reached a barely coordinated status with 3D urbanization, WSV reached a slightly coordinated status, while other indicators remained at the edge of being uncoordinated (Fig. 5a and Supplementary Fig. S24).

Specifically, concerning the coupling coordination relationship between 3D urbanization and the total ESV, most urban agglomerations experienced an increase in tele-CCD from 2005 to 2020, except for CC, QZ, and CY. Spatially, similar to intra-CCD and peri-CCD results, PRD, GFZC, and BG were observed to have relatively high tele-CCD values, generally at barely or slightly coordinated states. In contrast, HE, LX, CZYRN, and TNS exhibited lower tele-CCD values—though still higher than their intra-CCD and peri-CCD—remaining at slightly uncoordinated or at the edge of being

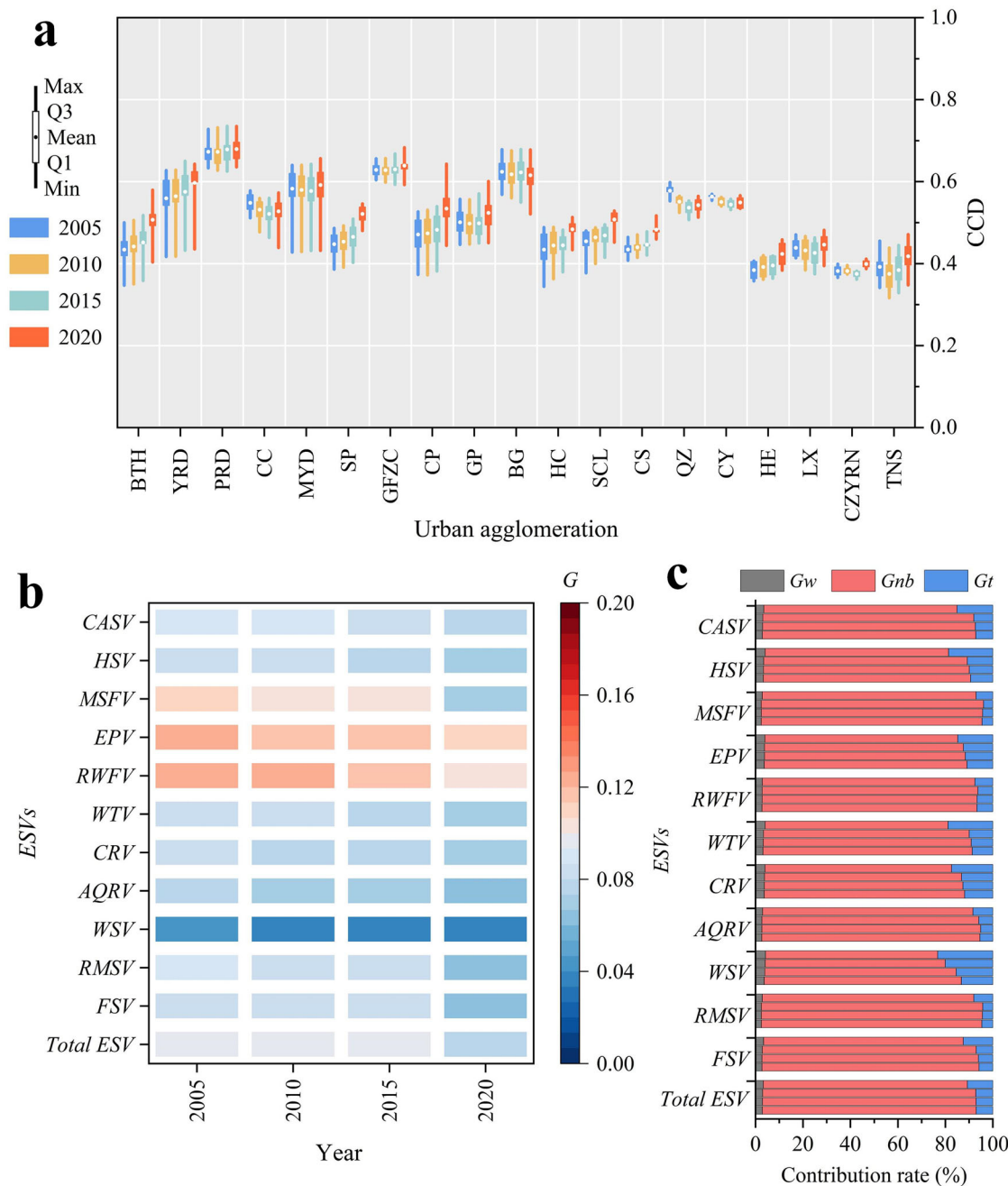


Fig. 5 | Tele-CCD between 3D urbanization and ESVs in China's urban agglomerations. **a** The changes of tele-CCD between 3D urbanization and the total ESV in different urban agglomerations (see Supplementary Fig. S24 for the results of other service indicators). **b** The temporal trends of overall Gini coefficients measuring tele-CCD differences between multiple ESVs and 3D urbanization across

urban agglomerations. **c** The sources of differences and the changes of contribution rates for tele-CCD, with results for 2005, 2010, 2015, and 2020 shown from bottom to top in each service categories. The full names are provided in Supplementary Table S1.

uncoordinated (Fig. 5a). Furthermore, the tele-CCD between multiple service indicators and 3D urbanization in most urban agglomerations has been achieved at the edge of being uncoordinated or barely/slightly coordinated status, though slightly lower than their peri-CCD. However, HE, LX, CZYRN, and TNS mainly remained slightly uncoordinated, but their tele-CCD values were marginally higher than peri-CCD and exhibited gradual improvement over time. Notably, similar to the trend of peri-CCD, declines were observed for multiple services in CC and QZ, as well as for FSV, RMSV, and MSFV in urban agglomerations such as PRD, MYD, GEZC, BG, and CY (Supplementary Fig. S24).

Moreover, the *G* of tele-CCD between multiple ESVs and 3D urbanization was generally lower than that of intra-CCD and peri-CCD. Among

them, RWFV, EPV, and MSFV displayed relatively notable differences, but all remained below 0.121 and consistently narrowed during the study period (Fig. 5b). Further decomposition of the Gini coefficients revealed that G_{nb} is the main source of *G*, generally contributing more than 72.51%. However, the contribution of differences within urban agglomerations (G_w) and transvariation (G_t) to overall differences gradually increased (Fig. 5c).

Discussion
Urban dynamic expansion from a 3D perspective

This study constructed a 3D urbanization intensity index that integrates horizontal and vertical dimensions and applied it to 19 major urban agglomerations in China. The results demonstrate a consistent upward

trend in 3D urbanization, accompanied by pronounced spatial heterogeneity. While earlier studies focusing on horizontal urban expansion have highlighted the rapid and irreversible spread of impervious surfaces since the economic reforms^{31,32}, our findings show that incorporating the vertical perspective can more comprehensively reflect the multidimensional characteristics of urbanization progress and regional differences. For instance, although northern urban agglomerations such as BTH, SP, and CP exhibit strong horizontal growth, their 3D urbanization lags behind that of southern agglomerations such as GFZC and MYD, once vertical building height growth is considered. This phenomenon reflects notable differences in urbanization development patterns between northern and southern China, which may be shaped by terrain, climate, economic development patterns, and industrial structures^{33,34}.

Additionally, our study found that regions with initially higher 3D urbanization values, such as QZ and CC, experienced declines despite continued increases in horizontal urbanization. This pattern suggests that urban expansion in these areas may have been dominated by low-rise horizontal growth. Numerous studies have demonstrated that China's urban expansion is increasingly "going uphill"³⁵, particularly in mountainous regions such as QZ and CC, where "slope climbing" urbanization has become more pronounced³⁶. This phenomenon refers to the trend of construction land gradually spreading into high-altitude, steep-slope areas to meet the demand for urban expansion. However, factors such as rugged terrain, unstable geological conditions, and higher infrastructure costs in mountainous regions pose major challenges to construction and development³⁷. Moreover, mountain ecosystems are highly fragile, and excessive urban encroachment may trigger environmental issues such as soil erosion and geological hazards^{38,39}. Consequently, urbanization in these regions may tend to horizontal expansion with predominantly low-rise buildings, leading to insufficient vertical urbanization—or even regression—thereby contributing to the decline in 3D-UUI values.

Meta-coupling framework for 3D urbanization and ecosystem service relationships

Urbanization and ES exhibit complex relationships that encompass both conflict and coordination⁴⁰. To more accurately capture the ecological consequences of urban growth, this study comprehensively considers both horizontal expansion and vertical development. Horizontal urbanization primarily drives land conversion and spatial sprawl, thereby influencing provisioning and supporting services by altering land use and ecosystem area. In contrast, vertical urbanization reshapes urban form, density, and energy exchange processes, affecting regulating services such as climate moderation and air purification, as well as cultural services through changes in visual landscapes and accessibility. This approach will provide a more comprehensive understanding of how different aspects of urban growth jointly alter the structure and functions of ecosystems^{19,20}.

Generally speaking, in the early stages of urbanization, some cities may prioritize expansion at the expense of ecological degradation, generating pressure on ES and resulting in a conflicting relationship. However, with increasing ecological awareness and policy interventions, urbanization and ES can achieve positive coupling, forming more coordinated symbiotic relationships⁴¹. In our analysis, ESVs did not completely follow or diverge from the steady upward trajectory of 3D urbanization but instead showed fluctuations over time. For instance, the total ESV first declined but then rebounded slightly by 2020. These shifts may be associated with multiple interacting drivers, including ecological restoration programs, the implementation of environmental regulations, and adjustments in land-use planning that improved certain regulating and supporting services. However, it should be noted that pressures from urban expansion, industrial restructuring, and agricultural intensification may offset these gains, resulting in unstable trends³. Moreover, the relationship between urbanization and ESVs has long transcended local boundaries, reflecting tele-coupling effects across regions. Especially, as horizontal and vertical urbanization intensifies, it generates increasing demands for construction materials, energy, and ecosystem goods (e.g., timber, minerals, and water),

much of which is sourced from distant areas. This process externalizes environmental costs and degrades ES in resource-supplying regions. Conversely, environmental regulations or ecological restoration in one urban region can reduce pollutant exports or demand pressures, indirectly improving ES elsewhere^{25,26,42}.

To investigate this relationship, this study constructed a coupling coordination analysis framework based on meta-coupling theory. The advantage of this framework lies in its ability to capture not only localized coupling (e.g. intra-coupling within cities) but also multi-scale, multi-level relationships—including regional coupling (peri-coupling among cities within an urban agglomeration) and cross-regional linkages (tele-coupling between cities of different urban agglomerations), which provides a more comprehensive understanding of the dynamic characteristics and coordination pathways between 3D urbanization and ESVs. In this framework, urbanization was measured through both horizontal (impervious surface expansion) and vertical (building height growth) dimensions, while ecological conditions were evaluated by 11 service indicators and their total ESV. Additionally, the CCD theory and IDW algorithm were applied to measure system coupling intensity. While prior studies^{43,44} have also used similar methods, their focus was limited to local and distant relationships. Based on the meta-coupling theory, this study further incorporated urban agglomerations into the analysis framework, thereby allowing for a more comprehensive examination of the coupling relationships that shape coordinated development in the urbanization process.

However, this framework has limitations. It primarily emphasizes land-based urbanization and fails to incorporate multidimensional urbanization features such as population growth, economic development, and social change, which may affect the research conclusions^{45,46}. In addition, methodologically, while the equivalent factor method used in the dataset provides a practical tool for assessing and comparing of ESVs, it relies on land-cover-based coefficients rather than process-based ecological modeling. Consequently, biophysical mechanisms underlying services are not explicitly represented, and the results should be interpreted as indicative rather than strictly causal⁴⁷. Similarly, this study does not directly quantify material, energy, or information flows, which constrains the ability to capture feedbacks and spatial heterogeneity in urbanization - ES interactions. To address these limitations, we employed the CCD model, which characterizes the degree of interaction and coordinated development between subsystems by considering their coupling intensity and development status²¹. Embedding CCD within a meta-coupling framework links local, regional, and cross-regional dynamics, offering a simple yet systematic way to track coupling trends, even when process-level data are unavailable. Nevertheless, future research should pay more attention to the process-based ecological models and methods such as material flow, energy flow, and information entropy to more comprehensively disentangle the drivers, feedback mechanisms, and cross-scale dynamics of urbanization - ES relationships^{48,49}.

Coupling coordination between 3D urbanization and ecosystem services and recommendations for future synergistic development

The intra-CCD analysis reveals that most cities and urban agglomerations in China have gradually improved in coupling coordination between multiple ESVs and 3D urbanization. However, regions such as CC and QZ exhibited declines, suggesting the urban expansion—particularly into ecologically fragile mountainous areas—may accelerate ES degradation and weaken coordination. Supporting this interpretation, recent studies in these regions show that land-use conflicts are concentrated in built-up and peripheral zones and are strongly driven by human activities, highlighting how rapid development intensifies ecological stress⁵⁰. To address these challenges, urban planning in these regions should shift from extensive urban expansion toward compact and resilient growth strategies that balance development needs with ecological safeguards. Specific measures include strengthening slope protection and ecological restoration in high-risk zones, promoting vertical urbanization where topography permits to reduce

horizontal sprawl, and adopting stricter zoning regulations to limit construction in ecologically sensitive areas^{38,39}.

Furthermore, spatially, the intra-CCD demonstrates notable differences, with higher levels in the east and south. This is mainly because southeastern regions, such as the PRD and YRD, enjoy favorable natural endowments, including a warm and humid climate, fertile soils, and dense river networks, which provide a strong ecological foundation⁵¹. Meanwhile, rapid economic growth, advanced urban planning, and stronger governance capacity, as well as long-standing practices in ecological restoration and green infrastructure, enable these regions to achieve a more advanced coordination⁵². Notably, several western and northern cities exhibit low intra-CCD, with 3D urbanization surpassing local ES despite lower urbanization levels. In these regions, dynamic monitoring of urbanization and ecological carrying capacity is crucial. Stricter land-use and urban planning regulations should be implemented to control excessive expansion, while financial and policy incentives could promote ecosystem restoration and green infrastructure. By contrast, southeastern urban agglomerations should prioritize maintaining their advanced coordination through continuous ecological investment, innovation in green technologies, and adaptive governance mechanisms^{51,53}.

The peri-CCD analysis indicates that the coupling coordination relationship between 3D urbanization and multiple ESVs in most urban agglomerations range from at the edge of being uncoordinated to slightly coordinated. Particularly in certain eastern urban agglomerations (e.g., the PRD) have achieved moderately coordinated or well-coordinated. In contrast, central and western urban agglomerations (e.g., HE, LX, CZYRN, and TNS) exhibit lower peri-CCD values, where both urbanization development and ES provision remain underdeveloped, leaving these regions on the brink of imbalance. Consequently, these patterns suggest the need for region-specific strategies. In high-performing urban agglomerations, policies could promote “smart growth” through low-carbon urban design, vertical greening, and ecological infrastructure networks^{15,16}. For underperforming urban agglomerations, priority should be given to strengthening economic foundations and improving basic infrastructure, while also maintaining parallel efforts in ecological restoration and strict environmental safeguards. Development activities in ecologically sensitive areas should be tightly restricted, while degraded ecosystems require targeted rehabilitation programs such as wetland recovery, reforestation, and soil stabilization. Equally important, mechanisms to enhance intra-agglomeration interactions, such as coordinated land-use planning, joint ecological compensation schemes, and cross-city infrastructure networks, should be established to reduce uneven development and establish more effective synergistic mechanisms^{17,22,24}.

The tele-CCD results indicate that, on average, the coupling coordination between multiple ESVs and 3D urbanization is slightly higher across China’s urban agglomerations than their intra-CCD and peri-CCD. However, high-performing urban agglomerations (e.g., such as PRD, GFZC, and BG) exhibit slightly lower tele-CCD values than their intra-CCD and peri-CCD, while underperforming urban agglomerations (e.g., such as HE, LX, CZYRN, and TNS) exhibit the opposite pattern. This suggests that areas with weaker internal coordination often rely on cross-regional resource allocation, policy support, or ecological compensation to mitigate developmental deficiencies and enhance overall coordination. Prior studies further demonstrate that social-ecological interactions and optimized mobility across regions can strengthen ecosystem service synergies and improve metacoupling between urbanization and the ecological environment^{54,55}. Furthermore, the Dagum Gini and its decomposition coefficients further reveal a gradual narrowing of the overall CCD difference among China’s urban agglomerations during the study period. G_{nb} remains the main source of G , indicating notable differences across urban agglomerations. Meanwhile, the increasing contribution rates of G_w and G_t , particularly the steady increase of G_t , suggest strengthening inter-agglomeration interactions. These trends may reflect spillover effects from priority urbanization regions through industrial transfer and technology, as well as cross-regional ecological compensation mechanisms that support ecologically fragile regions⁵⁶. Consequently, future policies should prioritize strengthening

cross-regional cooperation mechanisms, including establishing comprehensive ecological compensation systems and industrial collaboration platforms. In practice, this could involve creating market-based ecological compensation schemes, setting up inter-provincial funds to support restoration in ecologically fragile regions, and encouraging joint planning of infrastructure and industrial layouts. More importantly, these measures should be implemented to maximize the radiating effects of high-CCD urban agglomerations, foster synergistic development between 3D urbanization and ESVs across regions, and ultimately create a virtuous cycle^{54,57}.

Conclusion

Drawing on a CCD framework based on meta-coupling theory, this study examined the spatiotemporal evolution of 3D urbanization and ESVs across 19 major urban agglomerations in China and analyzed their coupling coordination dynamics and differences. The main conclusions are as follows:

- (1) From 2005 to 2020, China’s urban agglomerations experienced notable spatiotemporal differentiation in 3D urbanization. Horizontally, urban agglomerations expanded rapidly, with the average HUII increasing from 0.038 to 0.087. Vertically, building height growth was modest and in some cases declining. As a result, the average 3D-UUI increased from 0.225 to 0.266, with regions such as CC and QZ even experiencing decreases. Spatially, cities in the southeastern coastal regions and the Yangtze River Basin (e.g., Shenzhen and Shanghai) exhibited higher 3D urbanization, while northern and western cities (e.g., Huyanghe and Hainan Tibetan Autonomous Prefecture) lagged, reflecting notable regional imbalances.
- (2) Multiple ESVs displayed a “U-shaped” trajectory. For instance, the average total ESV declined from 7.860 billion yuan/km² in 2005 to 7.511 billion yuan/km² in 2015, before recovering to 7.707 billion yuan/km² by 2020. However, certain services, such as FSV, RWFV, and MSFV, showed persistent declines. Spatially, eastern and southern urban agglomerations (e.g., PRD, GFZC, and BG) generally maintained higher ESV levels, while western and northern urban agglomerations (e.g., HE, CZYRN, and TNS) remained lower.
- (3) The intra-CCD between multiple ESVs and 3D urbanization generally improved, though declines were observed in CC and QZ. Spatially, intra-CCD followed the pattern of east higher than west, south higher than north. The peri-CCD results revealed that most urban agglomerations remained at the edge of being uncoordinated or barely coordinated, with PRD achieving moderately coordinated or well-coordinated, while central and western urban agglomerations (e.g., HE, LX, CZYRN, and TNS) approached or reached imbalance. Additionally, the tele-CCD results, including the Gini coefficient and its decomposition results, revealed a notable CCD difference, with G_{nb} as the main source. Simultaneously, the rising contribution of G_t indicates that the coupling between urban agglomerations are playing an increasingly important role.

Methods

Study area

According to the National New Urbanization Plan (2014–2020) (www.gov.cn/zhengce/2014-03/16/content_2640075.htm), China has prioritized the development of 19 major urban agglomerations. These urban agglomerations, spanning eastern, central, and western China, form a “two vertical and three horizontal” urbanization strategy pattern, which reflects distinct regional characteristics and differentiation (Fig. 6). These urban agglomerations can be classified into different categories: The first tier—BTH, YRD, PRD, CC, and MYD—is designated for “optimized development.” Located primarily in coastal areas and the Yangtze River Economic Belt, these urban agglomerations cover just 10.4% of China’s land area but support 40.2% of its population and generate 56.5% of its national GDP. The second tier—SP, GFZC, CP, GP, and BG—is identified for “growing development.” These emerging agglomerations, concentrated in coastal and central regions, exhibit strong growth potential. The remaining urban agglomerations fall

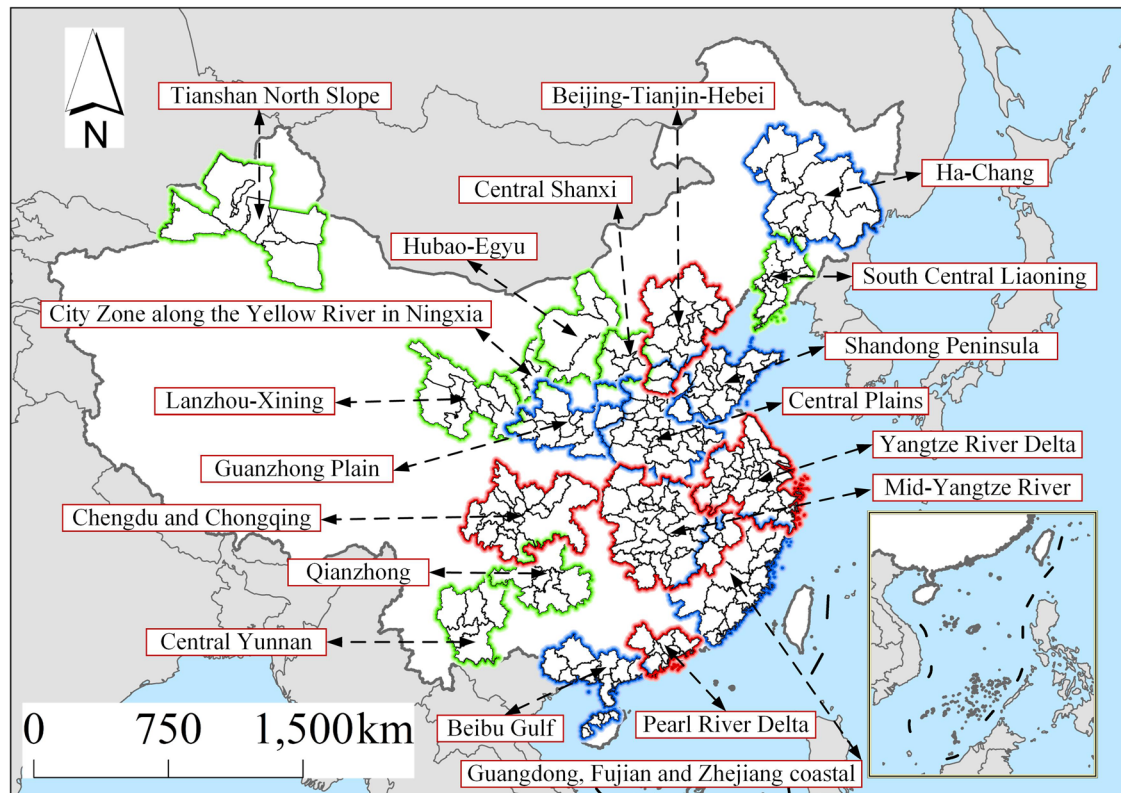


Fig. 6 | Schematic diagram of the study area. Our study area includes 19 major urban agglomerations in China: Beijing-Tianjin-Hebei (BTH), Yangtze River Delta (YRD), Pearl River Delta (PRD), Chengdu and Chongqing (CC), Mid-Yangtze River (MYD), Shandong Peninsula (SP), Guangdong, Fujian, and Zhejiang coastal (GFZC), Central Plains (CP), Guanzhong Plain (GP), Beibu Gulf (BG), Ha-Chang (HC), South Central Liaoning (SCL), Central Shanxi (CS), Qianzhong (QZ), Central Yunnan (CY), Hubao-Egyu (HE), Lanzhou-Xining (LX), City Zone along the Yellow River in Ningxia (CZYRN), and Tianshan North Slope (TNS).

under the “nurturing development” category. Located primarily in western China, these regions exhibit lower urbanization rates, fragmented spatial structures, weak economic linkages, and limited agglomeration effects⁵⁸.

However, the rapid urbanization of these agglomerations has led to increasingly severe ecological and environmental challenges. For instance, Beijing, the core city of BTH, has long suffered from atmospheric pollution, including persistent haze and PM_{2.5} concentrations⁵⁹. The YRD faces ecological pressures such as freshwater shortages and deteriorating water quality⁶⁰. Meanwhile, the PRD has experienced intensifying urban heat island effects and a notable increase in extreme heatwave events⁶¹. Agricultural regions also face distinct environmental burdens. Major grain-producing agglomerations, such as CP and SP, suffer from severe non-point source pollution due to excessive fertilizer and pesticide use⁶². Additionally, traditional industrial bases, including HC and SCL, face both atmospheric and water pollution challenges⁶³.

For research convenience, the spatial boundaries of our study were defined by including entire prefecture-level cities within urban agglomeration, even when only specific counties were officially designated (e.g., Fuzhou, Ji’an, Huizhou). Some cities are part of multiple agglomerations, such as Fuzhou, which belongs to both MYD and GFZC, and Heze, which belongs to both CP and SP. Finally, our study includes 241 cities across 19 urban agglomerations.

Data source and preprocessing

Urban impervious surface data. This study employed the annual global urban impervious surface (GAIA) data developed by Gong et al.⁶⁴ as the primary data source. The dataset provides a spatial resolution of 30 m, with validation accuracy exceeding 90% across multiple years, ensuring high reliability. To analyze the spatiotemporal dynamics of horizontal urbanization, we extracted impervious surface data for 2005, 2010, 2015, and 2020. All data processing—including mosaicking, projection

transformation, regional clipping, and resampling to 1 km—was conducted in ArcGIS software to generate a consistent time-series dataset covering the study area.

Urban building height data. Urban building heights were obtained from the 30 m China Multi-Temporal Built-up Height (CMTBH-30) dataset⁶⁵. This dataset was developed using a sample migration algorithm that integrates Global Ecosystem Dynamics Investigation (GEDI), Landsat, and PALSAR data through the Multi-Temporal Built-up Height estimation Network (MTBH-Net). Independent validations indicate robust performance, with root mean square errors consistently below 6.21 m across all surveyed years. Compared with previous products^{18,19}, CMTBH-30 provides multi-temporal coverage, enabling more accurate analysis of vertical urbanization dynamics. For this study, building height data for 2005, 2010, 2015, and 2020 were processed through projection transformation, regional clipping, and resampling to 1 km in ArcGIS software.

Ecosystem service value data. The ESVs data were sourced from the 1 km-resolution Spatial Distribution Dataset of Terrestrial Ecosystem Service Values in China developed by Xu et al.⁶⁶, which employed the equivalent factor method established by Xie et al.⁶⁷ to estimate 11 ESVs: Food Supply Values (FSV), Raw Material Supply Values (RMSV), Water Supply Values (WSV), Air Quality Regulation Values (AQRV), Climate Regulation Values (CRV), Waste Treatment Values (WTV), Regulation of Water Flows Values (RWFV), Erosion Prevention Values (EPV), Maintenance of Soil Fertility Values (MSFV), Habitat Services Values (HSV), and Cultural & Amenity Services Values (CASV), as well as the Total Ecosystem Service Values (total ESV). To analyze the spatiotemporal dynamics of ESVs in the study area, we selected data for 2005, 2010, 2015, and 2020. Preprocessing steps included projection

transformation, regional clipping, and exclusion of null-value urban areas in ArcGIS software.

Methods

This study systematically examined the coupling coordination relationships and spatiotemporal dynamics between 3D urbanization and ESVs across 19 urban agglomerations in China, employing a meta-coupling framework and CCD model (Fig. 7). Specifically, this study includes the following steps: First, we constructed a 3D urbanization intensity index by integrating horizontal impervious surface expansion with vertical building height growth, thereby quantifying the multidimensional dynamics of urbanization. Second, we applied time-series statistical and spatial analysis methods to examine the spatiotemporal evolution patterns of 11 ESVs and the total ESV. Third, building on the understanding of the reciprocal pressures and co-evolutionary between 3D urbanization and ESVs, this study applied meta-coupling theory to establish a multi-scale framework for analyzing urbanization—ES relationships. Fourth, the CCD model was incorporated to quantify the dynamic evolution and coupling coordination states between 3D urbanization and ESVs at different spatial scales, including intra-coupling (within individual cities), peri-coupling (within urban agglomerations), and tele-coupling (between different urban agglomerations). Finally, we employed the relative development model and Dagum Gini coefficient to conduct comparative analyses, examining both the relative development status of 3D urbanization and ESVs and regional disparities in their CCD relationships.

3D Urbanization assessment and spatiotemporal evolution analysis

For the horizontal dimension, this study utilized time-series GAIA data to calculate the proportion of impervious surface area within each city's administrative boundaries relative to the total area, thereby constructing the Horizontal Urbanization Intensity Index (HUII), which measures horizontal urbanization. For the vertical dimension, the study employed time-series CMTBH-30 data to calculate each city's average and maximum building height, and derived their ratio to establish the VUII, which measures vertical urbanization. To comprehensively capture the multidimensional dynamics of urban expansion, this study further integrated both horizontal and VUIIs to develop the 3D Urbanization Intensity Index (3D-UII). This composite index ranges from 0 to 1, with higher values indicating greater intensity of urbanization. The specific calculation formulas for HUII, VUII, and 3D-UII are presented below⁶⁸:

$$HUII = \frac{ISA}{BA} \quad (1)$$

$$VUII = \frac{BH_{mean}}{BH_{max}} \quad (2)$$

$$3D - UII = \alpha \times HUII' + \beta \times VUII' \quad (3)$$

Where ISA is the impervious surface area and BA is the total area of prefecture-level city; BH_{mean} and BH_{max} are the average and maximum building height, respectively; HUII' and VUII' represent the horizontal and VUIIs after range standardization, respectively. Given that horizontal and vertical urbanization are considered equally important in this study, coefficients were assigned as $\alpha = \beta = 0.5$ ⁶⁸.

Based on these formulas, we calculated the HUII, VUII, and 3D-UII for the years 2005, 2010, 2015, and 2020, revealing the development patterns and regional disparities of 3D urbanization across China's urban agglomerations.

Spatiotemporal evolution analysis of urban ecosystem service values

Based on time-series ESVs data, this study examined ES evolution characteristics. For the temporal dimension, we calculated descriptive

statistics—including maximum, minimum, mean values, and standard deviation—for all 11 ESVs and the total ESV at the city level from 2005 to 2020, thereby enabling a comparative analysis of ESVs change across different urban agglomerations. Furthermore, for the spatial dimension, ESVs distribution maps were generated for each urban agglomeration to reveal spatial differences.

A Meta-coupling framework for analyzing the relationship between 3D urbanization and ecosystem services

There are complex interactions between urbanization and ecosystem. On the one hand, urban expansion reduces natural ecological land (e.g., forests, grasslands, wetlands), directly weakening provisioning, regulating, and supporting services, while resource overconsumption and environmental pollution associated with urbanization further degrade ecosystem quality and stability^{69,70}. Beyond horizontal perspective, vertical urbanization imposes additional pressures by reshaping urban form, microclimates, and surface permeability. High-density urban development intensifies heat accumulation, disrupts wind and pollutant dispersion, accelerates storm-water runoff, and damages landscape connectivity, thereby affecting ES such as climate regulation, air purification, hydrological regulation, and habitat support^{18–20}. On the other hand, ES changes also feed back into urbanization processes. High-quality ES, such as clean air, sufficient water resources, and reliable food supply, provide the essential resource foundations and environmental safeguards that support economic growth and improve the quality of life during urbanization. Conversely, ES degradation, such as soil erosion and biodiversity loss, can constrain sustainable urbanization by elevating ecological risks, increasing development costs, and potentially triggering broader socioeconomic challenges (Fig. 8a)^{71,72}.

Notably, the relationship of urbanization and ES extends beyond local systems through cross-regional proximity and tele-coupling mechanisms⁷³. For instance, the offshoring of waste and polluting industries from developed countries to developing countries in Asia and Africa has caused severe soil and water contamination, resulting in ecosystem degradation⁷⁴. Similarly, China's South-North Water Transfer Project alleviates water scarcity in northern cities while imposing ecological costs on source regions, including altered hydrological regimes, wetland shrinkage, and biodiversity loss⁷⁵. These cases highlight how urbanization processes in one region can reshape ES dynamics in distant systems, underscoring the necessity of incorporating tele-coupling into urbanization - ES analyses.

Therefore, to systematically analyze these complex interrelationships, we developed a meta-coupling framework that integrates 3D urbanization and ESVs (Fig. 8b), building on Liu et al.'s^{27,28} meta-coupling theory. Within this framework, based on spatial scales and coupling scopes, we defined the coupling coordination relationship within individual cities as intra-coupling to reveal local-scale dynamics. Considering the frequent interactions and interdependencies among cities within urban agglomerations, we defined these relationships as peri-coupling to characterize regional-scale conflict and coordination effects. Furthermore, we defined the relationship that transcends urban agglomerations as tele-coupling to examine cross-regional coupling.

Assessment of coupling coordination relationships between 3D urbanization and ecosystem service values

To further investigate the coupling coordination relationship between 3D urbanization and ESVs, this study introduced the CCD model. Rather than modeling detailed biophysical processes or feedback flows, the CCD model enables the simultaneous assessment of each subsystem's development level and their degree of coordinated interaction, thereby providing a robust means to quantify the balance, conflicts, and synergies between different systems²¹. Therefore, building upon the meta-coupling framework and CCD model, this study examined intra-, peri-, and tele-coupling coordination to reveal the coupling coordination relationship between 3D urban expansion and ESVs across multiple spatial scales.

First, in the traditional CCD model, the coupling degree (C), coordination degree (T), and CCD between 3D urbanization and ESVs are

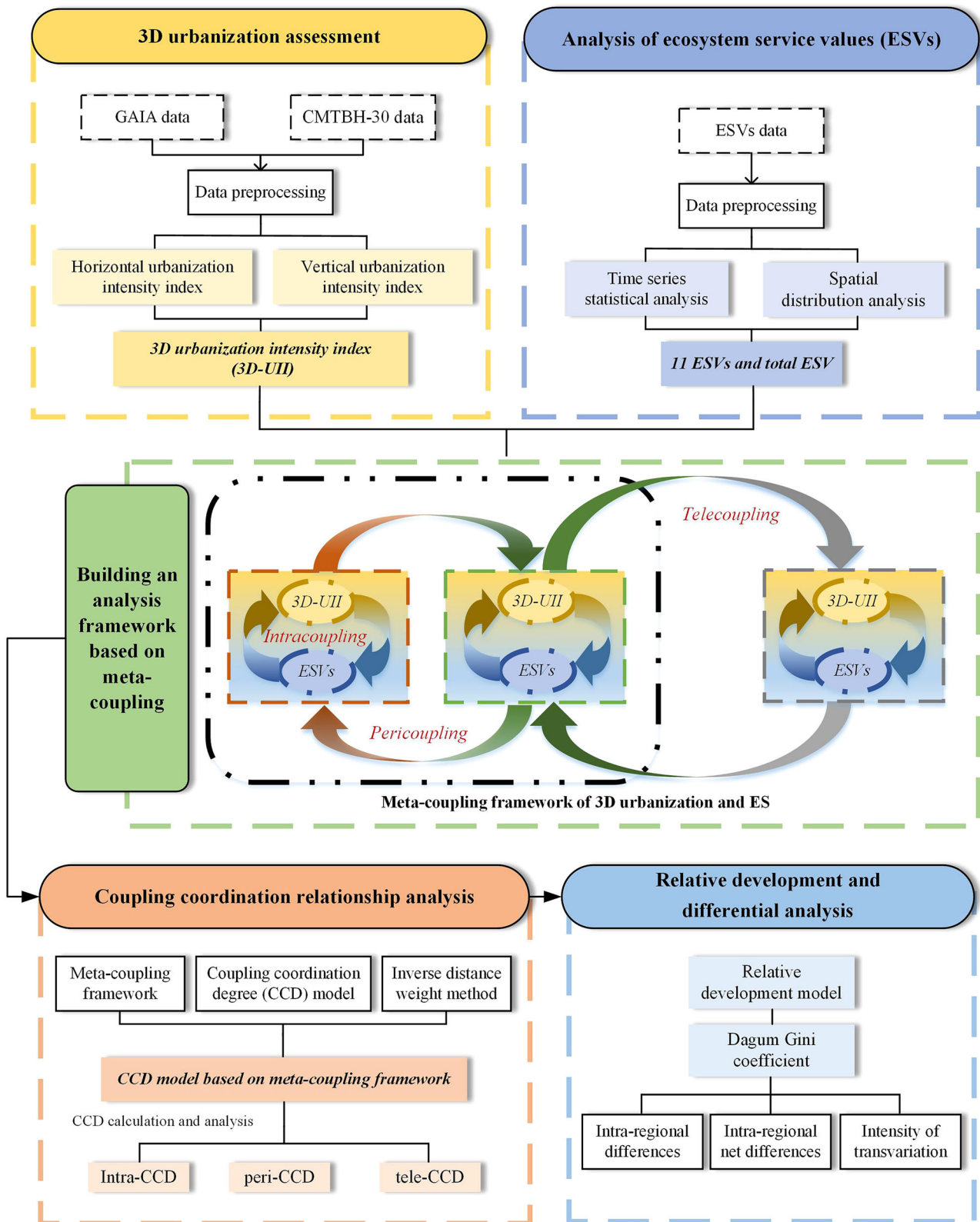


Fig. 7 | Technical roadmap. The workflow consists of: (1) assessing 3D urbanization by integrating horizontal and vertical expansion; (2) analyzing the spatiotemporal evolution of ecosystem service values; (3) developing a meta-coupling framework to examine cross-scale relationships between urbanization and ecosystem services; (4) quantifying coupling coordination dynamics at intra-, peri-, and tele-coupling scales; and (5) evaluating relative development patterns and regional disparities.

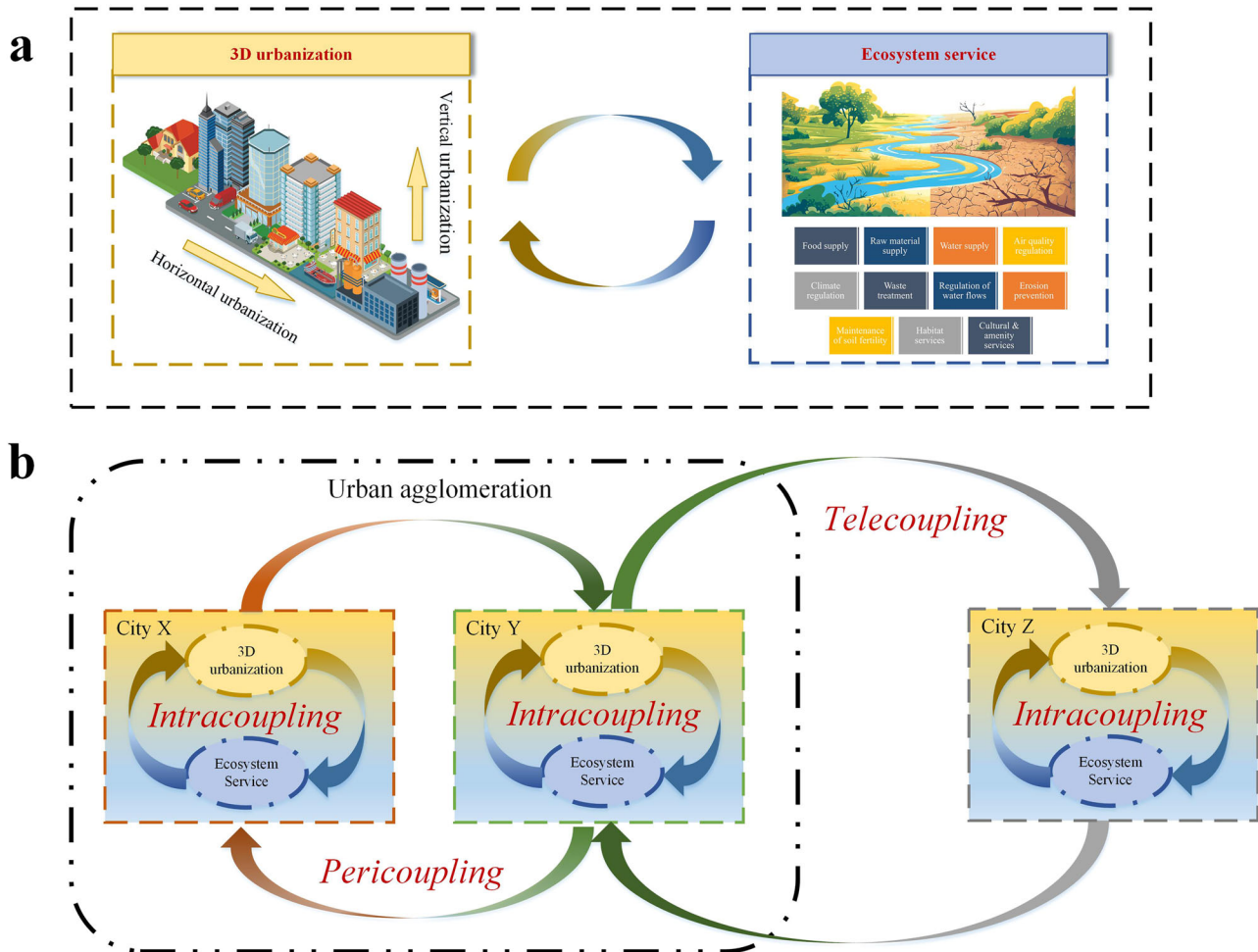


Fig. 8 | The meta-coupling framework for 3D urbanization and ecosystem services. To systematically analyze the complex coupling coordination relationships between 3D urbanization and ESVs, this study developed a meta-coupling analysis framework. **a** The framework integrates both horizontal and vertical dimensions of

urban expansion while incorporating all 11 ESVs and the total ESV. **b** Furthermore, to capture relationships across different spatial scales, the framework was divided into three domains: intra-coupling within local systems, peri-coupling among proximate systems, and tele-coupling across distant systems.

calculated as follows:

$$C = 2 \times \sqrt{\frac{U \times E}{(U + E)^2}} \quad (4)$$

$$T = \alpha \times U + \beta \times E \quad (5)$$

$$CCD = \sqrt{C \times T} \quad (6)$$

Where U is the degree of 3D urbanization, measured by the 3D-UII, while E is the ESVs, standardized to eliminate dimensional differences. Given the equal importance of urbanization and ES, the coefficients are set at $\alpha = \beta = 0.5$. Additionally, the CCD value ranges from 0 to 1, with higher values indicating greater coupling coordination.

Expanding on this model, we incorporated the Inverse Distance Weighting (IDW) method, following Tang et al.⁴⁵ and Xia et al.⁷⁶, to construct a CCD model within the meta-coupling framework. The C is defined as:

$$C_{ii} = C(U_i, E_i) \quad (7)$$

$$C_{Pi} = \frac{\sum_{j=1}^n \omega_{ij} \times C(U_i, E_j) + \sum_{j=1}^m \omega_{ij} \times C(U_j, E_i)}{2} \quad (8)$$

$$C_{Ti} = \frac{\sum_{k=1}^m \omega_{ik} \times C(U_i, E_k) + \sum_{k=1}^m \omega_{ij} \times C(U_k, E_i)}{2} \quad (9)$$

Where C_{ii} , C_{Pi} , C_{Ti} are intra-, peri-, and tele-coupling degrees, respectively. $C(U_i, E_i)$ is the coupling degree between 3D urbanization and ESVs in city i ; $C(U_i, E_j)$ is the coupling degree between 3D urbanization in city i and ESVs in city j , while $C(U_j, E_i)$ is the coupling degree between 3D urbanization in city j and ESVs in city i ; Similarly, $C(U_i, E_k)$ is the coupling degree between 3D urbanization in city i and ESVs in city k , while $C(U_k, E_i)$ is the coupling degree between 3D urbanization in city k and ESVs in city i . Cities j and i belong to the same urban agglomeration, whereas city k is part of another urban agglomeration. The variables n and m are the number of cities within city i 's urban agglomeration and outside of it, respectively. ω_{ij} and ω_{ik} are IDW values derived from an IDW matrix, calculated as follows:

$$\omega_{ij} = \frac{d_{ij}^{-p}}{\sum_{j=1}^n d_{ij}^{-p}} \quad (10)$$

$$\omega_{ij} = \frac{d_{ik}^{-p}}{\sum_{k=1}^m d_{ik}^{-p}} \quad (11)$$

Table 1 | CCD classification standards

Value range	Types
0.0–0.1	Extremely uncoordinated
0.1–0.2	Seriously uncoordinated
0.2–0.3	Moderately uncoordinated
0.3–0.4	Slightly uncoordinated
0.4–0.5	At the edge of being uncoordinated
0.5–0.6	Barely coordinated
0.6–0.7	Slightly coordinated
0.7–0.8	Moderately coordinated
0.8–0.9	Well-coordinated
0.9–1.0	Perfectly coordinated

Where d_{ij} and d_{ik} are the distances between the administrative centers of cities i and j and between cities i and k , respectively. The distance exponent p is set to 2, following existing research⁴⁵.

Similarly, the specific formula of coordination degree (T) is calculated as follows:

$$T_{ii} = T(U_i, E_i) \tag{12}$$

$$T_{Pi} = \frac{\sum_{j=1}^n \omega_{ij} \times T(U_i, E_j) + \sum_{j=1}^n \omega_{ij} \times T(U_j, E_i)}{2} \tag{13}$$

$$T_{Ti} = \frac{\sum_{k=1}^m \omega_{ik} \times T(U_i, E_k) + \sum_{k=1}^m \omega_{ik} \times T(U_k, E_i)}{2} \tag{14}$$

Where T_{ii} , T_{Pi} , T_{Ti} are intra-, peri-, and tele-coordination degrees, respectively. $T(U_i, E_i)$ is the coordination degree between 3D urbanization and ESVs in city i ; $T(U_i, E_j)$ is the coordination degree between 3D urbanization in city i and ESVs in city j , while $T(U_j, E_i)$ is the coordination degree between 3D urbanization in city j and ESVs in city i ; Similarly, $T(U_i, E_k)$ is the coordination degree between 3D urbanization in city i and ESVs in city k , while $T(U_k, E_i)$ is the coordination degree between 3D urbanization in city k and ESVs in city i .

Subsequently, the CCD values are then obtained as follows:

$$\text{intra - CCD} = \sqrt{C_{ii} \times T_{ii}} \tag{15}$$

$$\text{peri - CCD} = \sqrt{C_{Pi} \times T_{Pi}} \tag{16}$$

$$\text{tele - CCD} = \sqrt{C_{Ti} \times T_{Ti}} \tag{17}$$

Where intra-CCD, peri-CCD, and tele-CCD are intra-, peri-, and tele-coupling coordination degrees, respectively. Following the research by Nie and Lee⁷⁷, CCD values are classified into ten categories (Table 1).

Finally, based on the above models, this study quantified the spatio-temporal evolution characteristics of the coupling coordination relationships between 3D urbanization and 11 individual ESVs, as well as the total ESV, across urban agglomerations in 2005, 2010, 2015, and 2020.

Relative development and differential analysis

Our study introduced the relative development model, derived from ecological steady-state theory⁷⁸, to analyze 3D urbanization and ESVs. The model is expressed as follows:

$$R = \frac{U}{E} \tag{18}$$

Where R is the relative development degree, U represents 3D urbanization (measured by the 3D-UII), and E represents urban ecosystem service (expressed as ESVs after range standardization). When $R > 1$, ES development lags behind urbanization; when $R < 1$, urbanization lags behind ES development.

To further investigate the spatial differences and their sources in CCD across China’s urban agglomerations, this study employed the Gini coefficient and its decomposition method proposed by Dagum⁷⁹. Compared to traditional Gini coefficients and Theil indices, this method addresses sample overlap issues and decomposes the overall Gini coefficient (G) into intra-regional differences (G_w), inter-regional net differences (G_{nb}), and intensity of transvariation (G_t)⁸⁰. Specifically, the Dagum Gini coefficient is calculated as:

$$G = \frac{\sum_{j=1}^k \sum_{h=1}^k \sum_{i=1}^{n_j} \sum_{r=1}^{n_h} |y_{ji} - y_{hr}|}{2n^2\bar{y}} \tag{19}$$

Where n is the number of cities, and k is the number of subgroups, that is, the 19 urban agglomerations in this study; j and h are the number of subgroups divided, while i and r are the number of cities within the subgroup; n_j (n_h) is the number of cities within a subgroup of j (h), y_{ji} (y_{hr}) is the CCD of any city in a certain urban agglomeration, and \bar{y} is the average value of all CCDs.

Generally, a higher G value indicates greater imbalance in CCD differences. For decomposition, subgroups are first ranked by their average CCD values (Eq. 20):

$$\bar{y}_1 \leq \bar{y}_h \leq \dots \leq \bar{y}_j \leq \dots \leq \bar{y}_k \tag{20}$$

On this basis, G is decomposed into G_w , G_{nb} , and G_t . Here, G_w represents the CCD differences within an urban agglomeration, G_{nb} represents the CCD differences between different urban agglomerations, and G_t reflects the contribution rate of interactions between G_w and G_{nb} to the overall differences.

$$G_{jj} = \frac{\frac{1}{2Y_j} \sum_{i=1}^{n_j} \sum_{r=1}^{n_j} |y_{ji} - y_{jr}|}{n_j^2} \tag{21}$$

$$G_w = \sum_{j=1}^k G_{jj} \times p_j \times s_j \tag{22}$$

$$G_{jh} = \frac{\sum_{i=1}^{n_j} \sum_{r=1}^{n_h} |y_{ji} - y_{hr}|}{n_j n_h \times (\bar{Y}_j + \bar{Y}_h)} \tag{23}$$

$$G_{nb} = \sum_{j=2}^k \sum_{h=1}^{j-1} G_{jh} \times (p_j s_h + p_h s_j) \times D_{jh} \tag{24}$$

$$G_t = \sum_{j=2}^k \sum_{h=1}^{j-1} G_{jh} \times (p_j s_h + p_h s_j) \times (1 - D_{jh}) \tag{25}$$

Where G_{jj} is the Gini coefficient of CCD for urban agglomeration j , and G_{jh} is the Gini coefficient of CCD between urban agglomerations j and h ; \bar{Y}_j and \bar{Y}_h are the average CCD values of urban agglomerations j and h , respectively. The remaining variables are defined as:

$$P_j = \frac{n_j}{n}, P_h = \frac{n_h}{n}, S_j = \frac{n_j \bar{Y}_j}{n \bar{Y}}, S_h = \frac{n_h \bar{Y}_h}{n \bar{Y}}, D_{jh} = \frac{d_{jh} - P_{jh}}{d_{jh} + P_{jh}} = \frac{\int_0^\infty dF_j(y) \int_0^y (y-x) dF_h(x) - \int_0^\infty dF_j(y) \int_0^\infty (y-x) dF_h(x)}{\int_0^\infty dF_j(y) \int_0^\infty (y-x) dF_h(x) + \int_0^\infty dF_h(y) \int_0^y (y-x) dF_j(x)}$$

Finally, this study quantified both the relative development status between 3D urbanization and 11 ESVs, as well as the total ESV, and the

regional differences in their CCD across China's urban agglomerations in 2005, 2010, 2015, and 2020, using the relative development model and Dagum Gini coefficient.

Data availability

The GAIA (Annual Global Urban Impervious Surface) and CMTBH-30 (30-meter China Multi-Temporal Built-up Height) datasets used in this study are provided by the iEarth DataHub and are publicly available (<https://data-starcloud.pcl.ac.cn/iearthdata>). The 1 km-resolution Spatial Distribution Dataset of Terrestrial Ecosystem Service Values in China was obtained from the Resource and Environmental Science Data Platform and is publicly accessible (<https://www.resdc.cn/DOI/DOI.aspx?DOIID=48>).

Received: 11 July 2025; Accepted: 17 November 2025;

Published online: 04 February 2026

References

- Chen, L. & Zhang, A. Identification of land use conflicts and dynamic response analysis of Natural-Social factors in rapidly urbanizing areas –a case study of urban agglomeration in the middle reaches of Yangtze River. *Ecol. Indic.* **161**, 112009 (2024).
- Long, H. Theorizing land use transitions: a human geography perspective. *Habitat. Int.* **128**, 102669 (2022).
- Feng, X. et al. Impacts of land use transitions on ecosystem services: a research framework coupled with structure, function, and dynamics. *Sci. Total Environ.* **901**, 166366 (2023).
- Costanza, R. et al. The value of the world's ecosystem services and natural capital. *Nature* **387**, 253–260 (1997).
- Estoque, R. C. et al. Assessing environmental impacts and change in Myanmar's mangrove ecosystem service value due to deforestation (2000–2014). *Glob. Chang. Biol.* **24**, 5391–5410 (2018).
- De Groot, R. S., Alkemade, R., Braat, L., Hein, L. & Willemen, L. Challenges in integrating the concept of ecosystem services and values in landscape planning, management and decision making. *Ecol. Complex.* **7**, 260–272 (2010).
- Ma, Y. & Yang, J. A review of methods for quantifying urban ecosystem services. *Landsc. Urban Plan.* **253**, 105215 (2025).
- Foley, J. A. et al. Global consequences of land use. *Science* **309**, 570–574 (2005).
- Song, W. & Deng, X. Land-use/land-cover change and ecosystem service provision in China. *Sci. Total Environ.* **576**, 705–719 (2017).
- Yuan, Y. et al. Urban sprawl decreases the value of ecosystem services and intensifies the supply scarcity of ecosystem services in China. *Sci. Total Environ.* **697**, 134170 (2019).
- Xie, W., Huang, Q., He, C. & Zhao, X. Projecting the impacts of urban expansion on simultaneous losses of ecosystem services: a case study in Beijing, China. *Ecol. Indic.* **84**, 183–193 (2018).
- McPhearson, T., Andersson, E., Elmqvist, T. & Frantzeskaki, N. Resilience of and through urban ecosystem services. *Ecosyst. Serv.* **12**, 152–156 (2015).
- Fang, C. & Yu, D. Urban agglomeration: an evolving concept of an emerging phenomenon. *Landsc. Urban Plan.* **162**, 126–136 (2017).
- Zhao, Y., Wang, S., Ge, Y., Liu, Q. & Liu, X. The spatial differentiation of the coupling relationship between urbanization and the eco-environment in countries globally: a comprehensive assessment. *Ecol. Model.* **360**, 313–327 (2017).
- Zhai, Y. et al. Coupling coordination between urbanization and ecosystem services value in the Beijing-Tianjin-Hebei urban agglomeration. *Sustain. Cities Soc.* **113**, 105715 (2024).
- Ding, T., Chen, J., Fang, Z. & Chen, J. Assessment of coordinative relationship between comprehensive ecosystem service and urbanization: a case study of Yangtze River Delta urban Agglomerations, China. *Ecol. Indic.* **133**, 108454 (2021).
- Li, J. et al. Spatiotemporal differentiation of the ecosystem service value and its coupling relationship with urbanization: a case study of the Lanzhou-Xining urban agglomeration. *Ecol. Indic.* **160**, 111932 (2024).
- Huang, H. et al. Estimating building height in China from ALOS AW3D30. *ISPRS J. Photogramm. Remote Sens.* **185**, 146–157 (2022).
- Li, M., Koks, E., Taubenböck, H. & van Vliet, J. Continental-scale mapping and analysis of 3D building structure. *Remote Sens. Environ.* **245**, 111859 (2020).
- Taylor, P. D. Fragmentation and cultural landscapes: tightening the relationship between human beings and the environment. *Landsc. Urban Plan.* **58**, 93–99 (2002).
- Chen, P. & Shi, X. Dynamic evaluation of China's ecological civilization construction based on target correlation degree and coupling coordination degree. *Environ. Impact Assess. Rev.* **93**, 106734 (2022).
- Qiao, B., Fang, C. & Huang, J. The coupling law and its validation of the interaction between urbanization and eco-environment in arid area. *Acta Ecol. Sin.* **26**, 2183–2190 (2006). (in Chinese).
- Ai, J., Feng, L., Dong, X., Zhu, X. & Li, Y. Exploring coupling coordination between urbanization and ecosystem quality (1985–2010): a case study from Lianyungang City, China. *Front. Earth Sci. China* **10**, 527–545 (2016).
- Zhu, S., Huang, J. & Zhao, Y. Coupling coordination analysis of ecosystem services and urban development of resource-based cities: a case study of Tangshan city. *Ecol. Indic.* **136**, 108706 (2022).
- Grewal, S. S. & Grewal, P. S. Can cities become self-reliant in food?. *Cities* **29**, 1–11 (2012).
- Rudolph, A. & Figge, L. Determinants of ecological footprints: what is the role of globalization?. *Ecol. Indic.* **81**, 348–361 (2017).
- Liu, J. Integration across a metacoupled world. *Ecol. Soc.* **22**, 29 (2017).
- Liu, J. Leveraging the metacoupling framework for sustainability science and global sustainable development. *Natl. Sci. Rev.* **10**, nwad090 (2023).
- Asuncion, M. S. et al. Global invasion history of the fire ant *Solenopsis invicta*. *Science* **331**, 1066–1068 (2011).
- Jia, N. et al. The Russia-Ukraine war reduced food production and exports with a disparate geographical impact worldwide. *Commun. Earth Environ.* **5**, 765 (2024).
- Kuang, W., Liu, J., Zhang, Z., Lu, D. & Xiang, B. Spatiotemporal dynamics of impervious surface areas across China during the early 21st century. *Chin. Sci. Bull.* **58**, 1691–1701 (2013).
- Gong, P., Li, X. & Zhang, W. 40-Year (1978–2017) human settlement changes in China reflected by impervious surfaces from satellite remote sensing. *Sci. Bull.* **64**, 756–763 (2019).
- Yang, C. & Zhao, S. A building height dataset across China in 2017 estimated by the spatially-informed approach. *Sci. Data* **9**, 76 (2022).
- Yin, C. et al. Spatio-temporal evolution of urban built-up areas and analysis of driving factors—A comparison of typical cities in north and south China. *Land Use Policy* **117**, 106114 (2022).
- Zhou, L., Dang, X., Mu, H., Wang, B. & Wang, S. Cities are going uphill: Slope gradient analysis of urban expansion and its driving factors in China. *Sci. Total Environ.* **775**, 145836 (2021).
- Zhang, L. et al. Understanding the ecological impacts of vertical urban growth in mountainous regions. *Ecol. Inf.* **87**, 103079 (2025).
- Xu, K., Kong, C., Li, J., Zhang, L. & Wu, C. Suitability evaluation of urban construction land based on geo-environmental factors of Hangzhou, China. *Comput. Geosci.* **37**, 992–1002 (2011).
- Smyth, C. G. & Royle, S. A. Urban landslide hazards: incidence and causative factors in Niterói, Rio de Janeiro State, Brazil. *Appl. Geogr.* **20**, 95–118 (2000).
- Zhou, N. & Zhao, S. Urbanization process and induced environmental geological hazards in China. *Nat. Hazard.* **67**, 797–810 (2013).

40. Wang, J., Zhou, W., Pickett, S. T., Yu, W. & Li, W. A multiscale analysis of urbanization effects on ecosystem services supply in an urban megaregion. *Sci. Total Environ.* **662**, 824–833 (2019).
41. De Oliveira, J. A. P. Implementing environmental policies in developing countries through decentralization: the case of protected areas in Bahia, Brazil. *World Dev.* **30**, 1713–1736 (2002).
42. Pranindita, A., Teuling, A. J., Fetzer, I., & Wang-Erlandsson, L. Forests support global crop supply through atmospheric moisture transport. *Nat. Water.* **3**, 1243–1255 (2025).
43. Tang, P. et al. Local and telecoupling coordination degree model of urbanization and the eco-environment based on RS and GIS: a case study in the Wuhan urban agglomeration. *Sustain. Cities Soc.* **75**, 103405 (2021).
44. Han, Z. et al. Accounting for spatial coupling to assess the interactions between human well-being and environmental performance. *J. Clean. Prod.* **448**, 141666 (2024).
45. Liu, Z., Liu, S. & Song, Y. Understanding urban shrinkage in China: developing a multi-dimensional conceptual model and conducting empirical examination from 2000 to 2010. *Habitat. Int.* **104**, 102256 (2020).
46. Luo, J. et al. Coupling analysis of multi-systems urbanization: evidence from China. *Ecol. Indic.* **170**, 112977 (2025).
47. Zhang, Y., Zheng, H. & Chen, X. Effects of ecological restoration projects on ecosystem services flows. *Ecosyst. Serv.* **70**, 101681 (2024).
48. Decker, E. H., Elliott, S., Smith, F. A., Blake, D. R. & Rowland, F. S. Energy and material flow through the urban ecosystem. *Annu. Rev. Energy Env.* **25**, 685–740 (2000).
49. Cumming, G. S. et al. Implications of agricultural transitions and urbanization for ecosystem services. *Nature* **515**, 50–57 (2014).
50. Zhu, L. & He, Y. Mitigating spatial land use conflicts through an ecological lens: insights from the Chengdu-Chongqing urban agglomeration. *Environ. Dev. Sustain.* **27**, 1–24 (2025).
51. Zhang, W. et al. Long-term dynamic monitoring and driving force analysis of eco-environmental quality in China. *Remote Sens* **16**, 1028 (2024).
52. Luo, M., Zhou, Y., Sultan, M. S., Hakimjon, H. & Yu, Y. Spatiotemporal dynamics and driving factors of the coupling relationship between regional urban development and green space ecological quality. *Ecol. Indic.* **179**, 114009 (2025).
53. Wang, M., Krstikj, A. & Koura, H. Effects of urban planning on urban expansion control in Yinchuan City, Western China. *Habitat Int* **64**, 85–97 (2017).
54. Huang, Y. et al. Optimizing cross-regional mobility contributes to the metacoupling between urbanization and the environment for regional sustainability. *Land* **14**, 1682 (2025).
55. Han, Z. & Deng, X. The impact of cross-regional social and ecological interactions on ecosystem service synergies. *J. Environ. Manag.* **357**, 120671 (2024).
56. Zou, L., Liu, H., Wang, F., Chen, T. & Dong, Y. Regional difference and influencing factors of the green development level in the urban agglomeration in the middle reaches of the Yangtze River. *Sci. China Earth Sci.* **65**, 1449–1462 (2022).
57. Yang, W. & Lu, Q. Integrated evaluation of payments for ecosystem services programs in China: a systematic review. *Ecosyst. Health Sustain.* **4**, 73–84 (2018).
58. Sha, A., Zhang, J., Pan, Y. & Zhang, S. How to recognize and measure the impact of phasing urbanization on eco-environment quality: an empirical case study of 19 urban agglomerations in China. *Technol. Forecast. Soc. Change* **210**, 123845 (2025).
59. Liang, L., Wang, Z. & Li, J. The effect of urbanization on environmental pollution in rapidly developing urban agglomerations. *J. Clean. Prod.* **237**, 117649 (2019).
60. Fan, X. et al. Urbanization and water quality dynamics and their spatial correlation in coastal margins of mainland China. *Ecol. Indic.* **138**, 108812 (2022).
61. Tse, J. W. P. et al. Investigation of the meteorological effects of urbanization in recent decades: a case study of major cities in Pearl River Delta. *Urban Clim.* **26**, 174–187 (2018).
62. Hou, M., Cui, X., Xie, Y., Lu, W. & Xi, Z. Synergistic emission reduction effect of pollution and carbon in China's agricultural sector: Regional differences, dominant factors, and their spatial-temporal heterogeneity. *Environ. Impact Assess. Rev.* **106**, 107543 (2024).
63. Chang, B. et al. Analysis of trade-off and synergy of ecosystem services and driving forces in urban agglomerations in Northern China. *Ecol. Indic.* **165**, 112210 (2024).
64. Gong, P. et al. Annual maps of global artificial impervious area (GAIA) between 1985 and 2018. *Remote Sens. Environ.* **236**, 111510 (2020).
65. Chen, P. et al. Characterizing dynamics of built-up height in China from 2005 to 2020 based on GEDI, Landsat, and PALSAR data. *Remote Sens. Environ.* **325**, 114776 (2025).
66. Xu, X. Spatial distribution data set of terrestrial ecosystem service values in China. *Resour. Environ. Sci. Data Platf.* <https://doi.org/10.12078/2018060503> (2018).
67. Xie, G., Zhang, C., Zhen, L. & Zhang, L. Dynamic changes in the value of China's ecosystem services. *Ecosyst. Serv.* **26**, 146–154 (2017).
68. Ruan, L. et al. Measuring the coupling of built-up land intensity and use efficiency: an example of the Yangtze River Delta urban agglomeration. *Sustain. Cities Soc.* **87**, 104224 (2022).
69. Long, H., Liu, Y., Hou, X., Li, T. & Li, Y. Effects of land use transitions due to rapid urbanization on ecosystem services: implications for urban planning in the new developing area of China. *Habitat. Int.* **44**, 536–544 (2014).
70. Fang, C., Liu, H. & Li, G. International progress and evaluation on interactive coupling effects between urbanization and the eco-environment. *J. Geogr. Sci.* **26**, 1081–1116 (2016).
71. Russo, A., Escobedo, F. J., Cirella, G. T. & Zerbe, S. Edible green infrastructure: an approach and review of provisioning ecosystem services and disservices in urban environments. *Agric. Ecosyst. Environ.* **242**, 53–66 (2017).
72. Cao, Y., Kong, L., Zhang, L. & Ouyang, Z. The balance between economic development and ecosystem service value in the process of land urbanization: a case study of China's land urbanization from 2000 to 2015. *Land Use Policy* **108**, 105536 (2021).
73. Chen, W. & Chi, G. Urbanization and ecosystem services: the multi-scale spatial spillover effects and spatial variations. *Land Use Policy* **114**, 105964 (2022).
74. Zhang, Z. et al. Municipal solid waste management challenges in developing regions: a comprehensive review and future perspectives for Asia and Africa. *Sci. Total Environ.* **930**, 172794 (2024).
75. Yan, H. et al. A review of the eco-environmental impacts of the South-to-North Water Diversion: implications for interbasin water transfers. *Engineering* **30**, 161–169 (2023).
76. Xia, Z. et al. Disentangling the local coupling and telecoupling of urbanization and ecosystem services to reveal archetypical social-ecological interactions in urban agglomerations. *Land Degrad. Dev.* **33**, 3916–3939 (2025).
77. Nie, C. & Lee, C. C. Synergy of pollution control and carbon reduction in China: spatial-temporal characteristics, regional differences, and convergence. *Environ. Impact Assess. Rev.* **101**, 107110 (2023).
78. Zou, C., Zhu, J., Lou, K. & Yang, L. Coupling coordination and spatiotemporal heterogeneity between urbanization and ecological environment in Shaanxi Province, China. *Ecol. Indic.* **141**, 109152 (2022).
79. Dagum, C. A new approach to the decomposition of the Gini income inequality ratio. *Empir. Econ.* **22**, 515–531 (1997).
80. Han, H., Ding, T., Nie, L. & Hao, Z. Agricultural eco-efficiency loss under technology heterogeneity given regional differences in China. *J. Clean. Prod.* **250**, 119511 (2020).

Acknowledgements

This work was financially supported by the National Social Science Foundation of China [grant numbers 20ZDA085], the Natural Science Foundation of Shanghai [grant numbers 24ZR1440400] and the Technical Service Project of Shanghai Mengzhi Technology Co., Ltd. [grant numbers hx2025114].

Author contributions

Yinshuai Li: Conceptualization, Formal analysis, Methodology, Visualization, Writing—original draft. Nan Jia: Data curation, Methodology, Software, Writing—review and editing. Lilin Zheng: Software, Data curation, Investigation, Validation, Writing—review and editing, Funding acquisition. Chenglong Yin: Software, Data curation, Writing—review and editing. Kai Chen: Data curation, Investigation, Validation. Nansha Sun: Data curation, Investigation, Validation. Anyao Jiang: Data curation, Investigation, Validation. Mengting Wang: Validation, Funding acquisition, Writing—review and editing. Ruishan Chen: Project administration, Resources, Supervision, Writing—review and editing. Zhenju Zhou: Funding acquisition, Writing—review and editing.

Competing interests

The authors declare no competing interests.

Additional information

Supplementary information The online version contains supplementary material available at <https://doi.org/10.1038/s43247-025-03047-w>.

Correspondence and requests for materials should be addressed to Nan Jia or Ruishan Chen.

Peer review information *Communications Earth and Environment* thanks Alex Lechner and the other, anonymous, reviewer(s) for their contribution to the peer review of this work. Primary Handling Editors: C. Kendra Gotangco Gonzales, Yann Benetreau, and Mengjie Wang. A peer review file is available.

Reprints and permissions information is available at <http://www.nature.com/reprints>

Publisher's note Springer Nature remains neutral with regard to jurisdictional claims in published maps and institutional affiliations.

Open Access This article is licensed under a Creative Commons Attribution-NonCommercial-NoDerivatives 4.0 International License, which permits any non-commercial use, sharing, distribution and reproduction in any medium or format, as long as you give appropriate credit to the original author(s) and the source, provide a link to the Creative Commons licence, and indicate if you modified the licensed material. You do not have permission under this licence to share adapted material derived from this article or parts of it. The images or other third party material in this article are included in the article's Creative Commons licence, unless indicated otherwise in a credit line to the material. If material is not included in the article's Creative Commons licence and your intended use is not permitted by statutory regulation or exceeds the permitted use, you will need to obtain permission directly from the copyright holder. To view a copy of this licence, visit <http://creativecommons.org/licenses/by-nc-nd/4.0/>.

© The Author(s) 2026